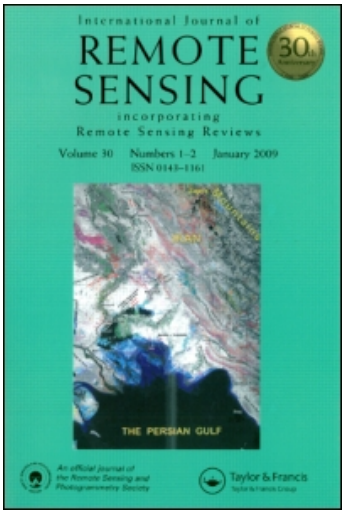

International Journal of Remote Sensing
Publication details, including instructions for authors and subscription information:
http://www.informaworld.com/smpp/title~content=t713722504

Combining close-range and remote sensing for local assessment of biophysical characteristics of arable land

G. W. A. M. van der Heijden[a]; J. G. P. W. Clevers[b]; A. G. T. Schut[c]
[a] Plant Research International, 6700 AA Wageningen, The Netherlands [b] Centre for Geo-Information (CGI), Wageningen University and Research Centre, 6700 AA Wageningen, The Netherlands [c] Curtin University of Technology, Perth, WA 6845, Australia

First published on: 20 June 2007

To cite this Article van der Heijden, G. W. A. M. , Clevers, J. G. P. W. and Schut, A. G. T.(2007) 'Combining close-range and remote sensing for local assessment of biophysical characteristics of arable land', International Journal of Remote Sensing, 28: 24, 5485 — 5502, First published on: 20 June 2007 (iFirst)
To link to this Article: DOI: 10.1080/01431160601105892
URL: http://dx.doi.org/10.1080/01431160601105892

International Journal of Remote Sensing
Vol. 28, No. 24, 20 December 2007, 5485–5502

Taylor & Francis
Taylor & Francis Group

Combining close-range and remote sensing for local assessment of biophysical characteristics of arable land

G. W. A. M. VAN DER HEIJDEN*†, J. G. P. W. CLEVERS‡ and A. G. T. SCHUT§

†Plant Research International, P.O. Box 16, 6700 AA Wageningen, The Netherlands
‡Centre for Geo-Information (CGI), Wageningen University and Research Centre, P.O. Box 47, 6700 AA Wageningen, The Netherlands
§Curtin University of Technology, GPO Box U1987, Perth, WA 6845, Australia

(*Received 21 February 2006; in final form 5 November 2006*)

For crop management, information on the actual status of the crop is important for taking decisions on nitrogen supply, water supply or harvesting. One would also like to take into account the local spatial variation of the crop. Remote sensing has proved to be a useful technique for estimating and mapping the spatial variation of various biophysical variables. Calibration of the image data is crucial in the performance and applicability of this technique. The aim of this paper is to show the possibility to calibrate remotely sensed imagery using fast and non-destructive close-range (below 1.3 m height) sensing instruments, thus providing a means for the assessment of plant characteristics over large areas at low costs. This concept was tested on a homogeneously managed grassland field, subdivided into 20 plots of 15×3 m, at the end of July 2004. Reflected radiation was recorded with an active close-range sensing device, consisting of a visible light and near-infrared (NIR) imaging spectrograph, and a 3CCD camera, equipped with special band filters (central wavelengths are at 600, 710 and 800 nm). An airborne campaign with a four-band UltraCam digital CCD camera was used for extrapolation to larger scales. Plots were harvested, and fresh and dry biomass and leaf nitrogen content were determined. Partial least squares (PLS) models combining spectral and spatial information from the close-sensing device yielded acceptable results in predicting grassland yields and nitrogen content. Subsequently, these predictions were used to calibrate a model with the image data of the remote sensing device. These were then compared, using leave-one-out cross-validation, with the measured field variables, and the model proved to have an acceptable predictive power.

1. Introduction

1.1 *Yield gap*

Energetically speaking, current agricultural cropping systems have low efficiency. Under Dutch growing conditions – with highly developed agricultural practices – still no more than 1% of the energy of the sun reaching the earth's surface is fixed in plant biomass (chemical energy in crops). If we can increase the efficiency, the same, or more, biomass can be produced in a smaller area of land, and large areas of land can be used for other purposes. This increase in efficiency can be considerable. For

*Corresponding author. Email: gerie.vanderheijden@wur.nl

International Journal of Remote Sensing
ISSN 0143-1161 print/ISSN 1366-5901 online
http://www.tandf.co.uk/journals
DOI: 10.1080/01431160601105892

example, the net yield of grassland is estimated at no more than 8.5 tonnes (t) dry matter (DM) yield per hectare (ha) on average each year (y), whereas the potential gross yield with the same agricultural practices on experimental plots is estimated at $15\,t\,DM\,ha^{-1}\,y^{-1}$. This difference between the potential and the realized yield of $6.5\,t\,ha^{-1}$ is often referred to as the 'yield gap'. Since the area of grassland in the densely populated Netherlands is over 1×10^6 ha, lowering the yield gap for grassland by only 10% (i.e. an increase of $0.65\,t\,ha^{-1}$) implies that an area of over 70,000 ha of land in the Netherlands can be used for other purposes, without losing any biomass production. However, at this moment, it is still not clear what causes this 'yield gap'. Insight into the causes is hampered by the lack of fast and accurate methods for measuring crop growth. Various techniques, such as imaging spectroscopy, are therefore being developed for measuring growth and determining the causes of this yield gap. To assess stagnation of growth and impending yield reduction on a large scale, the availability of timely, fast and accurate methods that can be applied over large areas of land is required.

Once we are able to timely measure possible yield reduction, we can try to use this information to optimize grassland management practices. Optimization of grassland here refers to high quality biomass production in order to maximize animal production (e.g. milk). If we can not only measure growth, but also estimate, for example, the amount of nitrogen left in the soil (which could be re-used), we can also use it for minimizing environmental impacts associated with fertilization. This environmental impact is becoming of increasing concern as shown by Nosengo (2003).

Furthermore, a mixture of grass and clover is more complex to manage than pure grass swards. It is aimed at taking into account the benefits of white clover in a grass sward, in particular, nitrogen fixation, high protein content, digestibility, mineral content and high intake (Abberton and Marshall 2005).

1.2 *Close-range sensing*

The role of imaging spectroscopy for the characterisation of grass swards was studied by Schut *et al.* (2003a, b, c, 2005). They explored the potential for growth monitoring, detection of nitrogen and drought stress, and assessment of dry matter yield, clover content, nutrient content, feeding value, sward heterogeneity and production capacity using a close-range imaging spectroscopy system applicable in the laboratory, or for mini-experiments. From this, a mobile system was developed for application to open-field experiments, the so-called 'Imspector Mobile' (Molema *et al.* 2003). This imaging platform consists of two imaging spectrometers, covering the spectral range of 440–960 nm (Imspector V9) and 850–1680 nm (Imspector N17), and a 3CCD camera, equipped with special band filters (central wavelengths 600, 710 and 800 nm). The platform is further equipped with artificial light sources, and thus can take measurements independent of external weather conditions. A combination of image parameters and hyperspectral reflectance curves derived from classified images can be used to estimate yields, nutrient contents and the feeding value of grass plots (Schut *et al.* 2006).

1.3 *Remote sensing*

Although the Imspector Mobile is a non-destructive and relatively fast measurement device, it is not suitable for monitoring large areas of grassland. Remote sensing has

proved to be a useful technique for estimating and mapping vegetation biophysical variables over large areas. Both statistical and physical methods have been used for describing the relationship between spectral measurements and biophysical variables. As an example, a whole range of vegetation indices has been developed for estimating variables like biomass, leaf area index and the fraction of absorbed photosynthetically active radiation for a range of vegetation types (Daughtry *et al.* 2000, Broge and Leblanc 2001, Haboudane *et al.* 2002, 2004, Thenkabail *et al.* 2002). For estimating leaf chlorophyll and nitrogen content, imaging spectroscopy has shown promising results (Clevers and Jongschaap 2001). However, calibration of the image data is crucial in the performance and applicability of this technique. Beeri *et al.* (2005) developed an alternative approach for using ground truth models for sugar beet N-credit and tested these models with satellite images.

Therefore, we try to combine the dedicated close-range sensing equipment with remote sensing techniques. By using the Imspector Mobile for calibrating the remote sensing data, we hope to be able to extrapolate the results to large areas of grassland. The idea is illustrated in figure 1, where the aim of the paper is indicated by the grey arrows at the top. Destructive and expensive measurements are used to calibrate the close-range sensing device, which in turn are used to calibrate remote sensing data. The whole flowchart indicates the processes of the different methods used in this paper. For further explanation of methods and symbols, see section 2.5 and table 6 later on.

The objective of this paper is first to test the potential of the close-range Imspector Mobile system for estimating biophysical variables of the grassland field with a grass/clover mixture. Therefore, the features measured with this device will be used to build a model to predict important biophysical characteristics of grassland. This validated model can then be used to gather ground truth information on a large scale, within a short time frame, with limited labour requirements, and at low costs, compared to chemical analysis.

Subsequently, a model will be built with the reflectances derived from UltraCam digital camera images as explanatory variables and the biophysical estimates of the close sensing device as response variables. The performance of the model can be tested by comparing the estimates of this model with the originally measured biophysical variables. This two-step calibration allows for a much more cost-effective approach than direct calibration. The model can be used for spatial extrapolation.

First, we will describe the field experiment and the chemical analysis used in this study. Next, we will describe the Imspector Mobile and some of the variables that can be extracted from this device. Then, we will use these variables to build models for predicting the biophysical features. Finally, we will use the predicted values from the Imspector Mobile to construct a model for the remote sensing data. This model will be used to extrapolate the results to large areas of grassland.

2. Materials and methods

2.1 *Field experiment and chemical analysis*

At the Droevendaal experimental farm in Wageningen (the Netherlands), a total of 20 plots were defined within a field with a mixture of grass and white clover. The 20 plots were 15 m long and 3 m wide with a spacing of approximately 10 m between the plots. After recording the spectral reflectance with various instruments, plots were

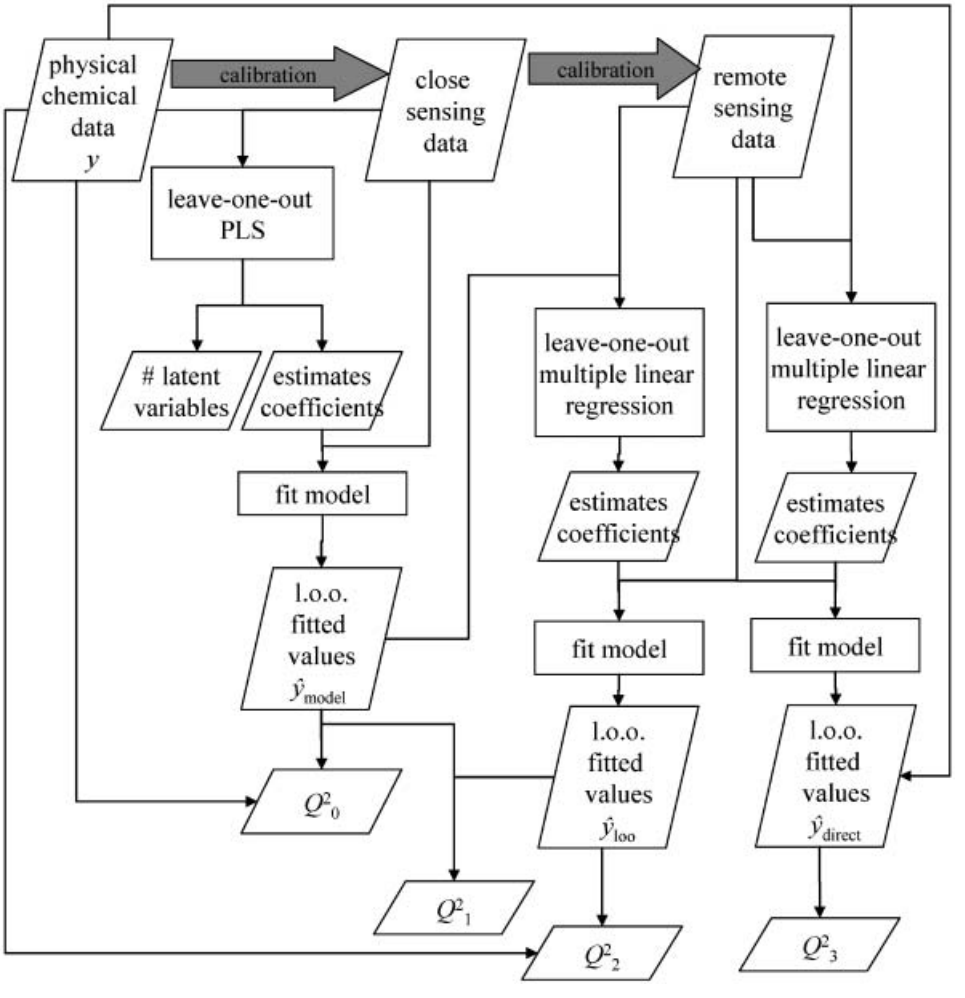

Figure 1. Flowchart showing the processes of the different methods used in this paper.

harvested with a plot-harvester on 30 July 2004. The biomass was recorded with a built-in weighing unit on the harvester. After cutting, a drill sample was taken from the harvested material. These samples were oven-dried for 72 hours at 70°C. After drying, samples were ground and sieved. From this material, a sub-sample was taken for wet-chemical analysis on total N, P, K, Ca and Na content. Total N and P content was measured with the so-called Segmented Flow Analysis procedure, after digestion with hydrogen peroxide, sulphuric acid, salicylic acid and selenium. Contents of K, Ca and Na were measured using Flame Atomic Emission Spectrometry.

2.2 *Imspector Mobile*

Reflectance values of individual plots were measured with the Imspector Mobile (shown in figure 2) on 29 July 2004. The Imspector Mobile has a GPS, a speedometer and three sensors on-board consisting of a detector, filters or spectrograph, a lens and an artificial xenon light source, which allows for

Figure 2. The Imspector Mobile containing two imaging spectrographs and a 3CCD camera in combination with artificial light.

nearly constant illumination over all recordings (Molema *et al.* 2003, Schut *et al.* 2006).

The three sensors are:

- A visible light imaging spectrograph (ImSpector V9). The V9 sensor records the reflection from 439–956 nm in 1090 spectral bands with 1300 pixels on the image line. The recorded image line at the soil surface is approximately 1.39 mm wide and 152 mm long.
- A NIR imaging spectrograph (ImSpector N17). The N17 sensor records the reflection from 848–1680 nm in 256 spectral bands with 320 pixels on the image line. The recorded image line at the soil surface is approximately 1.39 mm wide and 133 mm long.
- A 3CCD camera with 1024×1390 pixels and three narrow spectral bands at 600, 710 and 800 nm recording the reflection of an area of 45×60 cm on the soil surface. The wavelengths 600 and 710 nm were chosen since these are on both edges of the 680 absorption peak of chlorophyll, and are known to react to differences in N. The 800 nm wavelength provides a clear contrast between the crop and soil under the lamp characteristics and configuration used. Using image processing, the percentage of ground cover, an index of reflection intensity and the mean reflectances of green pixels per band were calculated from the 3CCD images. Within an image, the standard deviation of ground coverage was calculated over sub-blocks of 5 cm^2 and 15 cm^2. An example of a typical picture taken by this sensor is shown in figure 3.

One image line is taken such that it coincides with the upper part of the 3CCD image, the other image line coincides with the lower part of the 3CCD image, both across the 50% reflecting Spectralon standards. Images were recorded while driving with a velocity of 0.3–0.5 m s^{-1}. On each plot, 20–30 recordings were made with each sensor within a narrow strip of 60 cm wide in the middle of the plot. After recording,

Figure 3. Image from the 3CCD sensor from plot 1. (The 50% grey Spectralon standard is present at the top and bottom in every recording for internal calibration.)

reflectances were calculated using the Spectralon standard, available for every recording. The V9 and N17 images were warped to correct for bending in the spatial and spectral direction (van der Heijden and Glasbey 2003). All measurements were geo-located using the on-board GPS system.

2.3 *Extraction of explanatory variables from Imspector Mobile*

Three different sets of explanatory variables are measured with the Imspector Mobile. The first two sets of variables (referred to as X_{V9} and X_{N17}) are obtained from the spectroscopic measurements by the V9 and N17 spectrographs, respectively. For this, pixel spectra in the V9 and N17 spectrographs were normalized by dividing the spectrum by the mean reflectance from 743–955 nm for the V9 sensor, and from 1070–1130 nm for the N17 sensor. For V9, the spectrum was resampled at 3 nm resolution, from 451–949 nm, resulting in 167 variables. For N17, the spectrum was resampled at 6 nm resolution between 870–1596 nm, resulting in 122 variables.

The third set of features (referred to as X_{3CCD}) is extracted from images from the 3CCD camera. We use features that have shown good performance in previous experiments (Schut *et al.* 2006). Pixels in the images were classified into two classes: background material (soil, dead material) and green leaves (Schut *et al.* 2006). Ground coverage (*GC*) was calculated as the percentage of pixels classified as green material. The mean reflectance in bands at 600 (*R600*), 710 (*R710*) and 800 nm (*R800*) were calculated for pixels classified as green material.

As a result of the system design, reflection intensity is a function of leaf height and leaf angle. Higher reflection intensities correspond to higher positions in the canopy and a more horizontal leaf orientation. Therefore, pixels in the class with green leaves were subdivided into ten reflection intensity classes. The index of reflection intensity (*IRI*) is calculated as the percentage of pixels classified as green material that is present in the (intensity) classes with the highest reflection intensity (Schut *et al.* 2003a).

Schut *et al.* (2003a) used wavelet analyses and the spatial standard deviations to quantify heterogeneity, damage and productivity of grass swards. For the 3CCD images, a similar approach was followed. The 3CCD images were subdivided into square blocks of 5 cm^2 and 15 cm^2. The (spatial) standard deviation of *GC* values (*GC_SSD*) was calculated as the standard deviation of the *GC* values per block. Transects of 210 adjacent pixels were defined in the row and column direction within the 3CCD images. For each transect, wavelet entropy and wavelet energy values were calculated (Schut *et al.* 2003a). Finally, mean values per image and per plot were calculated. Wavelet entropy is a measure of the number of wavelet frequencies that are required to describe a certain pattern. Higher values for wavelet entropy correspond with grass dominated swards, and low values correspond with swards dominated by species with larger leaves (e.g. clover). The wavelet energy corresponds to the amplitude of a certain pattern; in our case, higher values coincide with more biomass accumulation. The clustering of green pixels with homogeneous colour characteristics was determined with image analyses procedures based on the principles of mathematical morphology. This procedure will result in a larger fraction of leaf clusters when swards are dominated by clover. In total, 20 features were extracted from the CCD images.

2.4 *UltraCam digital camera*

Vexcel's UltraCam digital camera system delivers large format aerial imagery that is radiometrically and geometrically superior to images captured by conventional film cameras at a comparable price (Schiewe 2005). It features a better than 12-bit per pixel dynamic range, compared to film cameras at less than 8-bits per pixel, and does not have any grain-noise. The UltraCam system comprises a panchromatic band and four multispectral bands as shown in table 1. On 28 July 2004, Aerodata performed a flight line across Wageningen with the UltraCam-D digital camera. The flight altitude was about 2790 m, resulting in a pixel size of 0.25 m for the panchromatic band, and 0.78 m for the multispectral bands (blue (*B*), green (*G*), red (*R*) and near-infrared (*NIR*)). Aerodata provided all data in tiff-format, after performing a geometric correction for the internal camera geometry and a radiometric correction for vignetting and white balance. In total, 21 images were recorded with an overlap of nearly 80%. The image size is given in table 1 in terms of pixels, which means that one image covers an area of about 2875 by 1875 m.

Figure 4 shows an example of parts of an UltraCam image over the Droevendaal trial field. Shadows of some cloud cover are present in the upper left corner of the image. Going further north along the flight line, the influence of cloud cover was becoming more severe. The UltraCam images were geo-referenced to the Dutch national coordinate system (RD) using a basemap. A second order polynomial transformation yielded an overall rms error of about 0.6 m using 97 ground control points. The pixel values of the UltraCam images can be converted to reflectance factors by using reference targets. A linear transformation can be used in order to

Table 1. Specifications of the UltraCam digital camera (Vexcel 2005).

Feature	Specification
Sensor type	Area CCD
Focal length (mm)	100 mm panchromatic 28 mm multispectral
Total field of view (°)	55×37
Number of CCD lines/camera	9
Panchromatic image size	11500×7500 pixels
Multispectral image size	3680×2400 pixels
Sensor size (μm)	9
Radiometric resolution (bit)	>12
Spectral resolution (nm)	450–665 (Pan)
(Full Width Half Maximum)	420–475 (blue) 455–580 (green) 635–675 (red) 700–805 (NIR)
Geo-referencing	POS Z/I 510 navigation system with GPS and INS

correct for camera calibration and atmospheric effects (Clevers 1988). The assumption is that effects (e.g. from the atmosphere) are the same for the targets and for the objects to be calibrated. Therefore, it is preferable to do this calibration to ground reflectances within one image if weather conditions are not optimal.

For this study, we had to relate the pixel values to the plot data. Using geo-referencing, we were able to locate the boundary of every plot in the remote sensing image (see figure 4). By taking the average pixel value within every plot (polygon) for each of the four bands, we could obtain four explanatory variables (*B*, *G*, *R*, *NIR*) for every plot.

Close study of the image revealed that plot 20 was at the edge of a cloud shadow. Therefore, this plot was excluded from further analysis using the UltraCam data, since the reflectance values of this plot were noticeably affected by the shadow cast.

2.5 *Statistical analysis*

As a first step, the variables measured by the Imspector Mobile were used as explanatory variables to estimate/predict the field-measured biophysical variables using partial least squares (PLS) models (Helland 1990). A PLS model relates the information of the sensors (*X*-block) to quantitative information of the measured variable of interest like biomass and N content (the *Y*-block, which can be univariate or multivariate). The PLS regression method effectively performs a canonical decomposition of the *X*-block in such a way that the resulting set of orthogonal factors are both predictive for the *Y*-block and describe as much as possible of the variance in the *X*-block. In this sense, PLS does not try to maximize correlation between *X* and *Y* (as is true for multiple linear regression) or the variance within *X* (like principal components analysis), but the covariance of *X* and *Y*. PLS is an iterative process where, in every iteration, scores, weights, loadings and inner-coefficients are calculated. Then, the *X*- and *Y*-block residuals are calculated, and the entire procedure is repeated for the next factor (commonly called a latent variable in PLS analysis). The error (expressed as the residual sum of squares) continues to decrease as the number of latent variables increases. However, the more latent variables are chosen, the more liable the model is to over-fitting. The optimal

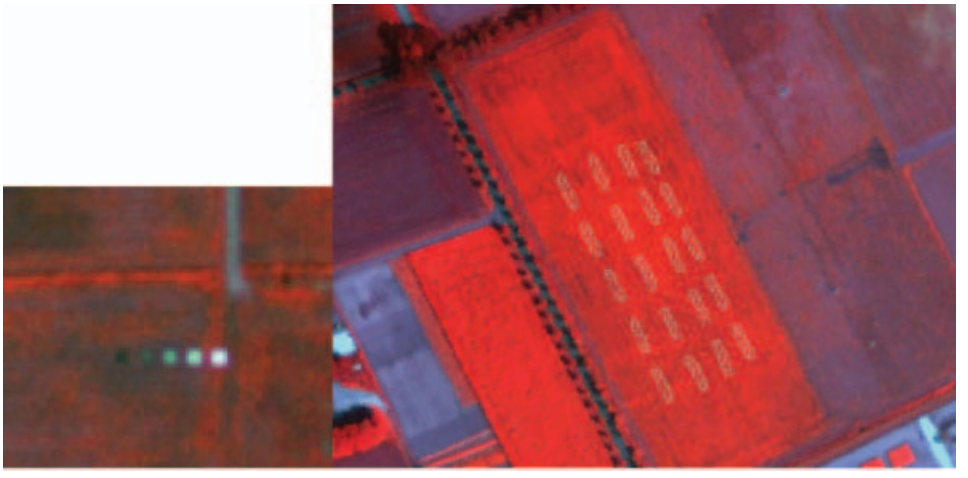

Figure 4. Parts of a false colour composite image made with the UltraCam-D camera over the Wageningen site on 28 July 2004 (image lvl02-00234). Left: part of the area with five reference targets is shown, right: the grass/clover test site with the polygons showing the Imspector measurement sites.

number of latent variables that is used to create the final PLS model is therefore generally determined by (leave-one-out) cross-validation.

Use of standard multiple linear regression can lead to highly unreliable coefficients of the model, when a number of explanatory variables are highly correlated. PLS is a linear model, which is especially useful when we have such highly correlated variables. It is therefore regularly used when dealing with spectroscopic data, and it also proved suitable for analysing the Imspector Mobile data (Schut *et al.* 2005, 2006).

For the PLS model, the number of latent variables has to be selected. As a measure of model performance, we used the root mean square error of cross-validation (*RMSECV*), which is calculated as:

$$RMSECV = \sqrt{\frac{\sum_i (y_i - \hat{y}_i)^2}{n}} \quad (1)$$

where y_i and $\hat{y}_i$ were the observed values and the leave-one-out predictions respectively of the variable of interest, i.e. the model was fitted without using observation i and then observation i was predicted using this model. This was carried out for all observations.

The number of latent variables in the model is determined as the lowest number of latent variables for which the *RMSECV* is not significantly different (α=0.10) from the overall minimum *RMSECV* using a randomization t-test (van der Voet 1994).

If the number of observations is low, and multiple explanatory variables are used in a model, we have to be careful for 'fitting to the noise'. We can easily obtain a model which has a nearly perfect fit (high R^2), but which, when applied to observations not used in fitting the model, gives very poor predictions. To obtain insight into the prediction ability of the model, we therefore prefer to use separate data for fitting and validating the model. However, since the number of observations is low, we do not want to set aside observations just for validation.

Therefore, leave-one-out cross-validation is often used in such cases to determine the prediction ability of the model, which gives a good estimate of the prediction ability with minimal loss of information when fitting the model.

In this study, the prediction ability of the model is measured as the proportion of variation accounted for by the model using leave-one-out cross-validation:

$$Q^2 = 1 - \frac{\sum_i (y_i - \hat{y}_i)^2}{\sum_i (y_i - \bar{y})^2} \tag{2}$$

where $\bar{y}$ is the average value of the observed variable of interest over the complete dataset, and y_i and $\hat{y}_i$ are again the observed values and the leave-one-out predictions of the variable. The Q^2 has strong resemblance with the familiar R^2, but can become negative if the prediction of the model is inadequate (e.g. in the case of over-fitting). The Q^2 is (as is R^2) strongly sensitive to the variation within the data set, so should be considered with caution. (The Q^2 for this first step (PLS model) is referred to as Q^2_0 in figure 1.)

Step two was to build a multiple linear regression (MLR) model using the predicted biophysical measurements from the first step ($\hat{y}_{\text{model}}$) as response variables, and the mean values of the calibrated reflectances, obtained with the UltraCam digital camera system coinciding with the measured area in the field, as explanatory variables:

$$\hat{y}_{\text{model}} = \beta_0 + \beta_1 B + \beta_2 G + \beta_3 R + \beta_4 NIR + \varepsilon, \tag{3}$$

where the β values are the coefficients to be estimated. B, G, R, NIR are the four explanatory variables and ε is the error of the model, assumed to be normally distributed with mean 0 and variance σ^2.

To obtain insight in the prediction performance of this model, we compare the leave-one-out predictions of this MLR model ($\hat{y}_{\text{loo}}$) with the predictions of step 1, leading to a Q^2 referred to as Q^2_1 in figure 1. Furthermore, we can compare $\hat{y}_{\text{loo}}$ with the true observations y, leading to Q^2_2 in figure 1.

As a third step, we can fit a MLR model directly to the biophysical features measured in the field:

$$y = \beta_0 + \beta_1 B + \beta_2 G + \beta_3 R + \beta_4 NIR + \varepsilon. \tag{4}$$

An indication of the performance of this model, again using leave-one-out predictions, is given by Q^2_3 in figure 1.

Finally, by using the model of step 2, we can use every pixel in the remote sensing image as a set of explanatory variables to predict for example biomass. This approach was used to extrapolate the field characteristics over the entire image.

3. Results

3.1 *Field measurements*

Table 2 summarizes the field measurements performed for the 20 plots of the grass/clover experiment. Yield figures were at a high level for all plots. The plots were defined within a normal grassland field, and no treatment differences existed between the various plots. As a result, the range in yield figures is not large, which

Table 2. Summary statistics for the 20 plots of the grass/clover experiment (harvested on 30 July 2004).

	Minimum	Maximum	Mean	Standard deviation	CV
Biomass ($t\,ha^{-1}$)	10.91	24.39	17.79	3.39	0.19
DM yield ($kg\,ha^{-1}$)	2186	4187	3346	499	0.15
DM content (%)	16.24	21.33	18.96	1.11	0.06
N content ($g\,kg^{-1}$ DM)	27.78	32.61	30.27	1.23	0.04

CV, coefficient of variation.

may reduce the statistical significance of relationships between spectral measurements and the field measurements.

3.2 *Close sensing: Imspector Mobile*

Table 3 gives the correlation coefficients of the most important image parameters and the four grassland characteristics: biomass, DM yield, DM content and N content. The variables *GC* and *GC_SSD* are most strongly correlated with biomass. Variability within a plot is negatively related to biomass, a larger heterogeneity means lower yields. Leaf clustering and wavelet entropy do not correlate strongly to any of the variables. Given the previously established relationships between leaf clustering, wavelet entropy and white clover content, this indicates that the content of white clover is not so important for differences in yield or contents between plots.

The spatial patterns and heterogeneity within the plots is illustrated in figure 5 for four variables derived from the 3CCD images of the Imspector Mobile. This figure clearly shows the heterogeneity within a plot.

3.3 *Remote sensing: UltraCam images*

After geometrically linking the Imspector Mobile measurements with the UltraCam images using the GPS data, a polygon matching the location of the Imspector measurements was defined for each plot (see figure 4). Table 4 summarizes the reflectances within the polygons of the four spectral bands. Also from these values,

Table 3. Correlation coefficients of the most important image parameters and biomass, DM yield, DM content and N content.

	Biomass	DM yield	DM content	N content
GC	0.85	0.75	−0.81	0.52
GC_SSD_5cm²	−0.59	−0.50	0.59	−0.40
GC_SSD_15cm²	−0.87	−0.78	0.78	−0.39
Leaf clusters	−0.04	−0.20	−0.26	0.14
Wavelet entropy	0.17	0.28	0.11	−0.13
R600/R710	−0.82	−0.77	0.71	−0.59
IRI	0.78	0.69	−0.76	0.50
(R800–R600)/(R800–R710)	−0.82	−0.70	0.81	−0.51
R600	−0.19	−0.20	0.11	−0.14
R710	0.32	0.28	−0.34	0.23
R800	0.80	0.69	−0.80	0.56

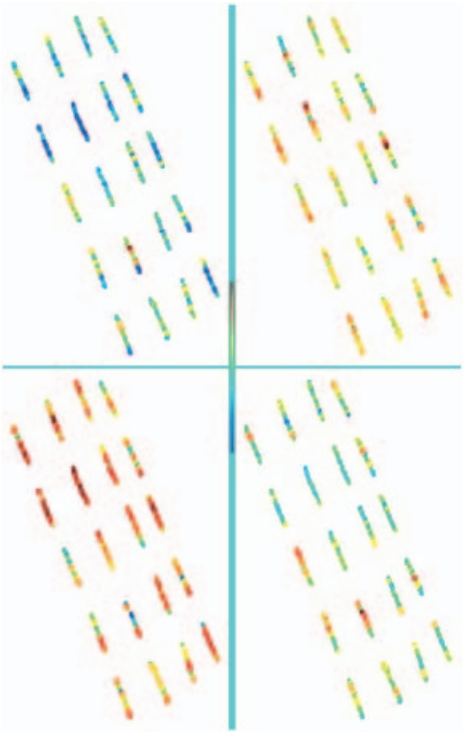

Figure 5. Colour plot with the spatial pattern of some variables derived by the Imspector. Top left: *GC_SSD_5cm*^{2}, top right: fraction of leaf clusters, bottom left: ground coverage, and bottom right: relative values of leaf colour (reflection @ 600 nm/reflection @ 710 nm).

we must conclude that the variation between the plots is very limited for the blue, green and red spectral bands.

3.4 *Statistical models*

In table 5, PLS models are presented for the fit of grassland characteristics versus two different sets of close sensing (Imspector Mobile) variables. The selected number of latent vectors using the randomization t-test was only one for all models. This is mainly due to the limited number of objects in this study.

The model that included only the feature set X_{3CCD} was most accurate for biomass, DM yield and DM content. For N content, none of the models performed

Table 4. Summary statistics of the UltraCam spectral reflectances for the 19 plots of the grass/clover experiment (harvested on 30 July 2004).

	Minimum	Maximum	Mean	Standard deviation	CV
Blue reflectance	0.0206	0.0266	0.0232	0.0019	0.08
Green reflectance	0.0361	0.0416	0.0386	0.0017	0.04
Red reflectance	0.0212	0.0281	0.0244	0.0022	0.09
Near-infrared reflectance	0.5433	0.6909	0.6084	0.0373	0.06

Table 5. Q^2 ($=Q^2_0$ in figure 1) and root mean square error of cross-validation (*RMSECV*) values of the PLS models.

	Biomass (t ha^{-1})		DM yield (kg ha^{-1})		DM content (%)		N content (g kg^{-1} DM)	
Model	Q^2	*RMSECV*	Q^2	*RMSECV*	Q^2	*RMSECV*	Q^2	*RMSECV*
Model 1: Y=observed Explanatory= X_{3CCD}	0.72	1.75	0.50	343	0.59	0.69	0.07	1.16
Model 2: Y=observed Explanatory= X_{3CCD} X_{V9} X_{N17}	0.42	2.52	0.25	420	0.32	0.89	0.13	1.12

satisfactory, which is probably due to the low variability in the measured N content values. Including the feature sets X_{V9} and X_{N17} resulted in lower Q^2 and larger *RMSECV* values (except for N content). This is most probably due to the small number of observations.

The predicted values of Model 1, obtained by leave-one-out, were used as response variable (referred to as $\hat{y}_{\text{Model 1}}$) to fit a multiple linear regression model. By using the leave-one-out predictions of the PLS model, the observed value for each point is not used for training the model to predict this point, hence ensuring control to an over-optimistic prediction. The average values of the blue, green, red and near-infrared pixels corresponding to the field plots at the geo-referenced positions were used as the explanatory variables (X-block). The fit of the MLR model is again expressed in terms of Q^2, i.e. using leave-one-out cross-validation and the corresponding root mean square error (*RMSE*).

As a reference, we also used the measurements as response variables and fitted a MLR model for the four bands. The percentage of variance explained by this model is again expressed using leave-one-out cross-validation (Q^2). For reference, we also provide R^2. Hence we have two measures for percentage of variance for the two-step model and one measure for the direct calibration. Results are shown in table 6 and figure 6.

In table 6, the leave-one-out predicted values of Model 1 ($\hat{y}_{\text{Model 1}}$) are used as response variables (two-step calibration) in columns 2–5. The goodness of fit is determined by comparing the leave-one-out predictions of the calibrated model ($\hat{y}_{\text{loo}}$) with either $\hat{y}_{\text{Model 1}}$ (columns 2 and 3), or the original measurements y (columns 4 and 5). Q^2 is the percentage of variation explained by this model, using leave-one-out cross-validation, *RMSE* is the corresponding root mean square error. In columns 6, 7 and 8, the model is fitted directly to the original measurements y. R^2 is the percentage of variance explained by the model using all data (i.e. no cross-validation). (See also figure 1 for the process of estimating $Q^2_{(1,2,3)}$.)

In figure 6, predicted versus measured values are shown for biomass, DM yield, DM content and N content. The predicted values for close sensing are obtained as fitted leave-one-out data of Model 1. The predicted values for remote sensing are obtained by fitting a MLR model using the fitted leave-one-out data of Model 1 as

Table 6. Results for fitting the multiple linear regression model with the plot values for the four bands of the remote sensing image as explanatory variables.

Model:	Calibration on $\hat{y}_{\text{Model 1}}$ Validation: $\hat{y}_{\text{loo}}$ versus $\hat{y}_{\text{Model 1}}$		Calibration on $\hat{y}_{\text{Model 1}}$ Validation: $\hat{y}_{\text{loo}}$ versus y		Calibration on y Validation: $\hat{y}$ (R^2) and $\hat{y}_{\text{loo}}$ versus y		
Variable	Q^2_1	$RMSE$	Q^2_2	$RMSE$	R^2	Q^2_3	$RMSE$
Biomass ($t\,ha^{-1}$)	0.62	1.81	0.65	1.94	0.77	0.54	2.24
DM yield ($kg\,ha^{-1}$)	0.62	250	0.61	301	0.68	0.42	368
DM content (%)	0.51	0.65	0.42	0.84	0.58	0.07	1.06
N content ($g\,kg^{-1}$)	0.36	0.60	0.24	1.07	0.35	−0.29	1.39

the response variables and the four spectral bands of the remote sensing data as the explanatory variables. The black line is the line $y=x$.

The UltraCam bands explain a reasonable proportion of the variability in the observed biomass and DM yield, using the predicted values from the close sensing

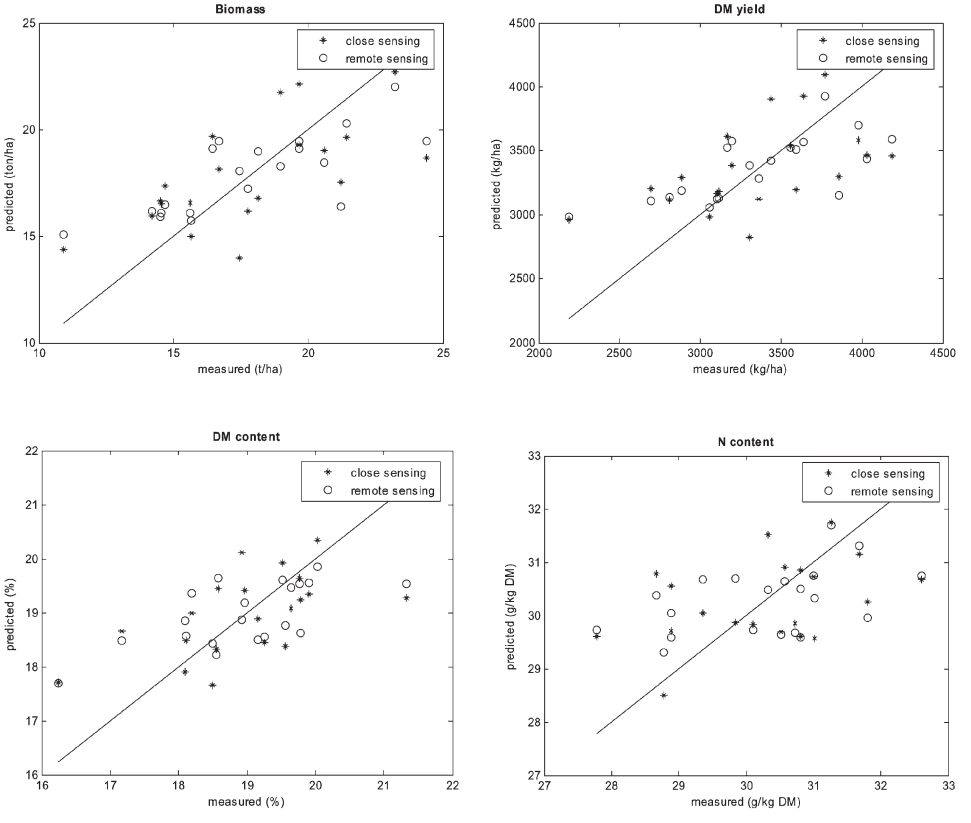

Figure 6. Predicted versus measured values for biomass, DM yield, DM content and nitrogen content.

device ($\hat{y}_{\text{Model 1}}$) as response variable. The direct fit of UltraCam variables on the observed values y was better in terms of R^2, but this is clearly over-optimistic as the same observation is used in both training the model and determining its performance. The R^2 is largely over-optimistic and does not give a good estimate of the generalisation power of the model, especially when using several explanatory variables (in this case four variables: *B*, *G*, *R*, *NIR*) and only a limited number of observations. The cross-validation as used here is therefore necessary.

It was hoped that the indirect fitting of the model using the close sensing data instead of the true measurements would not seriously deteriorate the model's performance. When comparing the *RMSE* values in columns 5 and 8 of table 6, the two-step calibration surprisingly gives a better result than the direct calibration. The MLR model can be applied to every pixel of the image. The extrapolation to the whole field is illustrated in figure 7.

4. Conclusions and discussion

The close-range sensing data, obtained by the Imspector Mobile, provided good estimates for biomass and DM yield and a reasonable estimate for the DM content. This is probably due to a good estimate of ground coverage and the height of the sward, using the detailed information in the 3CCD camera (Schut *el al.* 2003a).

The N content was not estimated well in this experiment. This was due to the limited size of the dataset and the limited observation range, since no special treatment was imposed on the plots. Therefore, the additional contribution of the spectrographs (V9, N17) in this experiment was limited. In other experiments, these proved to be very useful for measuring nutrients like N (Schut *et al.* 2003b, 2005, 2006).

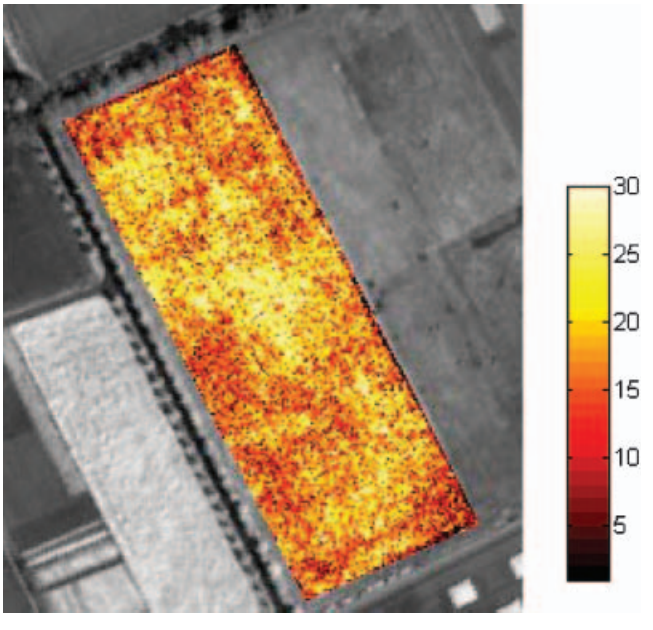

Figure 7. Spatial pattern of the predicted biomass (t ha^{-1}) for the grass/clover field at the Droevendaal experimental farm, Wageningen, the Netherlands.

As was shown in figure 5, the features measured with the Imspector Mobile showed considerable heterogeneity within a plot. Since the features were averaged over a plot, this variation within plots is lost, and only the variation between plots can be used to fit the model. The size of the plots was chosen equal to the size of plots used in previous trials (Schut *et al.* 2005, 2006), but from the heterogeneity shown in this figure, and the limited variation observed between the plots (table 2), it would have been preferable to use a larger number of smaller, more homogeneous plots. The size of the harvester, the size of the pixels, the accuracy of the geo-referencing and the amount of homogeneity should be taken into account to determine the optimal plot size, but this could have been considerably smaller, e.g. 3×3 m.

The small number of plots in this study limited the number of latent variables in the PLS model and reduced the calibration accuracy. The predictive performance of the model expressed as Q^2 and estimated with leave-one-out cross-validation is therefore probably underestimated for this field. How good the predictive performance would be for other fields is an interesting question and requires more research.

We have shown that it is possible to predict biomass, DM yield and DM content from remote sensing data through an indirect fit of closely sensed data with the Imspector Mobile. In this study, results were even better than through a direct fit, but the study was performed on only a limited number of objects and no firm conclusions can be drawn.

An explanation for this result may be due to the flexible and adequate fit of the PLS model, with features which have been proved suitable in earlier experiments, and which show a good linear relationship with the remote sensing variables (both are optical methods largely using the same part of the electromagnetic spectrum). Also, the predictions $\hat{y}_{\text{Model 1}}$ do not contain the stochastic measurement error which is present in y, and might hence be better suitable for building a model, especially when using only a limited number of observations. It should however also be noted that the original measurements have been used to estimate $\hat{y}_{\text{Model 1}}$. Therefore, $\hat{y}_{\text{Model 1}}$ for plot i is not independent of the measurements y of the other plots. The cross-validation might also be slightly biased by this.

Nevertheless, the results give confidence that an indirect method using a close-range sensing device can be used reliably for calibrating remote sensing images. This indirect calibration allows new ways for precision agriculture management and mapping of regional productivity over large areas since fast, non-destructive and reasonably accurate close-range sensing measurements can be used for calibrating remote sensing information at relatively low costs and low labour demands for gathering ground truth information.

The calibration of the Imspector Mobile is crucial for future applications. For this application, we used data from the field to calibrate the model, but it would be a serious advantage if calibration results from previous field data could be used. This may reduce the amount of ground truth data required even further. This is planned in future experiments.

The use of cross-validation for estimating the goodness of fit of the models is used in this study in order to prevent over-optimistic results. The risk of fitting-to-the-noise and poor generalisation of the model is high, especially when the number of explanatory variables is increasing, when traditional statistical methods like stepwise linear regression in combination with measures like R^2 or adjusted R^2 are used.

In a study by Yang *et al.* (2004), it was shown that grain sorghum yield variability could be explained for 69–82% using airborne hyper-spectral imaging. From a remote sensing point of view, it will be interesting to investigate whether the use of hyper-spectral imaging could further improve the predictive power of the remote sensing data, especially for features like dry matter content and N content. As a next step, it is planned to use airborne imaging spectrometry data for the extrapolation step.

Acknowledgements

We thank the 'Scheppen van Ruimte' programme for funding. We would like to acknowledge Aerodata for providing the UltraCam images and Vexcel for providing the specifications and spectral sensitivities of the UltraCam camera.

References

ABBERTON, M.T. and MARSHALL, A.H., 2005, Progress in breeding perennial clovers for temperate agriculture. *Journal of Agricultural Science*, **143**, pp. 117–135.

BEERI, O., PHILLIPS, R., CARSON, P. and LIEBIG, M., 2005, Alternate satellite models for estimation of sugar beet residue nitrogen credit. *Agriculture, Ecosystems and Environment*, **107**, pp. 21–35.

BROGE, N.H. and LEBLANC, E., 2001, Comparing prediction power and stability of broadband and hyperspectral vegetation indices for estimation of green leaf area index and canopy chlorophyll density. *Remote Sensing of Environment*, **76**, pp. 156–172.

CLEVERS, J.G.P.W., 1988, Multispectral aerial photography as a new method in agricultural field trial analysis. *International Journal of Remote Sensing*, **9**, pp. 319–332.

CLEVERS, J.G.P.W. and JONGSCHAAP, R.E., 2001, Imaging spectrometry for agricultural applications. In *Imaging Spectrometry: Basic Principles and Prospective Applications*, F.D. Van der Meer and S.M. De Jong (Eds), pp. 157–199 (Dordrecht: Kluwer Academic Publishers).

DAUGHTRY, C.S.T., WALTHALL, C.L., KIM, M.S., BROWN DE COLSTOUN E. and MCMURTREY III J.E., 2000, Estimating corn leaf chlorophyll concentration from leaf and canopy reflectance. *Remote Sensing of Environment*, **74**, pp. 229–239.

HABOUDANE, D., MILLER, J.R., PATTEY, E., ZARCO-TEJADA, P.J. and STRACHAN, I.B., 2004, Hyperspectral vegetation indices and novel algorithms for predicting green LAI of crop canopies: modeling and validation in the context of precision agriculture. *Remote Sensing of Environment*, **90**, pp. 337–352.

HABOUDANE, D., MILLER, J.R., TREMBLAY, N., ZARCO-TEJADA, P.J. and DEXTRAZE, L., 2002, Integrated narrow-band vegetation indices for prediction of crop chlorophyll content for application to precision agriculture. *Remote Sensing of Environment*, **81**, pp. 416–426.

HELLAND, I.S., 1990, Partial least squares regression and statistical models. *Scandinavian Journal of Statistics*, **17**, pp. 97–114.

MOLEMA, G.J., MEULEMAN, J., KORNET, J.G., SCHUT, A.G.T. and KETELAARS, J.J.M.H., 2003, A mobile imaging spectroscopy system as tool for crop characterization in agriculture. In *Fourth European Conference on Precision Agriculture*, 15–18 June 2003, Berlin (Wageningen NL: Wageningen Academic Publishers), pp. 499–500.

NOSENGO, N., 2003, Fertilized to death. *Nature*, **425**, pp. 894–895.

SCHIEWE, J., 2005, Status and future perspectives of the application potential of digital airborne sensor systems. *International Journal of Applied Earth Observation*, **6**, pp. 215–228.

SCHUT, A.G.T. and KETELAARS, J.J.M.H., 2003a, Assessment of seasonal dry-matter yield and quality of grass swards with imaging spectroscopy. *Grass and Forage Science*, **58**, pp. 385–396.

SCHUT, A.G.T. and KETELAARS, J.J.M.H., 2003b, Imaging spectroscopy for early detection of drought stress in grass swards. *Netherlands Journal of Agricultural Science*, **51**, pp. 319–337.

SCHUT, A.G.T. and KETELAARS, J.J.M.H., 2003c, Imaging spectroscopy for early detection of nitrogen deficiency in grass swards. *Netherlands Journal of Agricultural Science*, **51**, pp. 297–317.

SCHUT, A.G.T., LOKHORST, C., HENDRIKS, M.M.W.B., KORNET, J.G. and KASPER, G.J., 2005, Potential of imaging spectroscopy as tool for pasture management. *Grass and Forage Science*, **60**, pp. 34–45.

SCHUT, A.G.T., VAN DER HEIJDEN G.W.A.M., HOVING, I., STIENEZEN, M.W.J., VAN EVERT, F.K. and MEULEMAN, J., 2006, Imaging spectroscopy for on-farm measurement of grassland yield and quality. *Agronomy Journal*, **98**, pp. 1318–1325.

THENKABAIL, P.S., SMITH, R.B. and DE PAUW, E., 2002, Evaluation of narrowband and broadband vegetation indices for determining optimal hyperspectral wavebands for agricultural crop characterization. *Photogrammetric Engineering and Remote Sensing*, **68**, pp. 607–621.

VAN DER HEIJDEN G.W.A.M. and GLASBEY, C.A., 2003, Calibrating spectral images using penalized likelihood. *Real-Time Imaging*, **9**, pp. 231–236.

VAN DER VOET H., 1994, Comparing the predictive accuracy of models using a simple randomization test. *Chemometrics and Intelligent Laboratory Systems*, **25**, pp. 313–323.

VEXCEL, 2005, Available online at: http://www.vexcel.com/products/photogram/ultracam/ (accessed 20 January 2006).

YANG, C., EVERITT, J.H. and BRADFORD, J.M., 2004, Airborne hyperspectral imagery and yield monitor data for estimating grain sorghum yield variability. *Transactions of the ASAE*, **47**, pp. 915–924.